Volume 43 | Number 7 | 21 February 2014 | Pages 2697–3006

Dalton Transactions

An international journal of inorganic chemistry

www.rsc.org/dalton

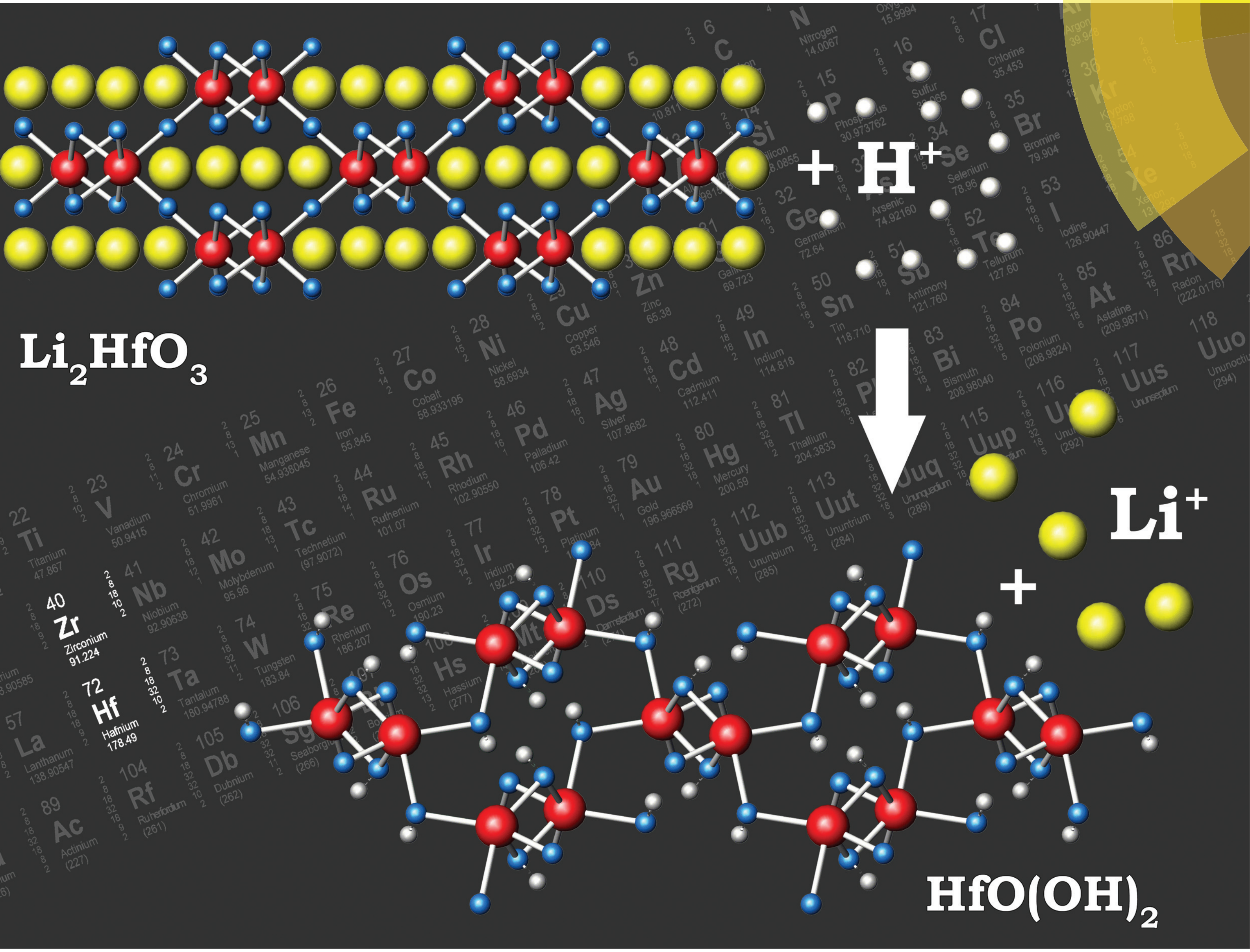

ISSN 1477-9226

ROYAL SOCIETY OF CHEMISTRY

COVER ARTICLE
Tarakina *et al.*
Synthesis and characterisation of new $MO(OH)_2$ (M = Zr, Hf) oxyhydroxides and related Li_2MO_3 salts

Dalton Transactions

PAPER

View Article Online
View Journal | View Issue

Cite this: Dalton Trans., 2014, 43, 2755

Synthesis and characterisation of new $MO(OH)_2$ (M = Zr, Hf) oxyhydroxides and related Li_2MO_3 salts

Yana V. Baklanova,[a] Tatyana A. Denisova,[a] Lidiya G. Maksimova,[a] Alexander P. Tyutyunnik,[a] Inna V. Baklanova,[a] Igor R. Shein,[a] Reinhard B. Neder[b] and Nadezda V. Tarakina*[a,c]

Received 16th October 2013, Accepted 1st December 2013

DOI: 10.1039/c3dt52929k

www.rsc.org/dalton

Two new solid $MO(OH)_2$ (M = Zr, Hf) oxyhydroxides have been synthesised by an ion-exchange reaction from Li_2MO_3 (M = Zr, Hf) precursors obtained by a citrate combustion technique. The crystal structure of the oxyhydroxides has been solved by direct methods and refined using Rietveld full profile fitting based on X-ray powder diffraction data. Both oxyhydroxides crystallize in a $P2_1/c$ monoclinic unit cell and have a structure resembling that of the related salts. Detailed characterisation of the fine-structure features and chemical bonding in precursors and oxyhydroxide powders has been performed using vibrational spectroscopy, nuclear magnetic resonance spectroscopy, scanning electron microscopy, pair distribution function analysis and quantum-chemical modelling.

Introduction

Solid oxyhydroxides have been intensively studied from the point of view of both fundamental science and potential applications. Natural oxyhydroxides (goethite, akaganeite, lepidocrocite, diaspore, boehmite and other minerals)[1–4] and synthetic oxyhydroxides of 3d-transition metals (NiOOH, FeOOH, MnOOH, *etc.*) attract most of the attention because of their potential as materials for electrochemical energy storage,[5–11] sensors,[12] absorbents[13,14] and electrochromic devices.[15–17]

However, in spite of active research in this field, there are only a few reports concerning the synthesis and the characterisation of solid oxyhydroxides of the 4th group of the periodic table. Orera *et al.* reported on the synthesis of $ZrO(OH)_2\cdot 0.14H_2O$ oxyhydroxide from Li_2ZrO_3 salt in an aqueous solution of nitric acid.[18] Denisova *et al.* described a method of synthesis and some properties of metatitanic acid H_2TiO_3.[19] Yawata reported on recovering lithium ions from hot spring water using H_2TiO_3, obtained from Li_2TiO_3 by an ion exchange reaction.[20] Recently, we showed that all three $MO(OH)_2$ (M = Ti, Zr, Hf) oxyhydroxides can be synthesised in solid form by an ion exchange reaction in aqueous acetic acid solution from Li_2MO_3 (M = Ti, Zr, Hf) precursors.[19,21–23] It is worth mentioning that the precursors in ref. 19–23 have been obtained by standard solid-state synthesis at temperatures 600–700 °C,[19,21] which are significantly lower than the temperatures used during the solid-state synthesis of the above-mentioned lithium salts.[24–30] In the case of $TiO(OH)_2$ we showed that decreasing the synthesis temperature is crucial for obtaining oxyhydroxides. Indeed, only precursors annealed at low temperatures allow the complete exchange of Li^+ by H^+ (the extent of exchange of lithium by protons in Li_2TiO_3 obtained at 800–1000 °C was found to be less than 50%).[21,22] We proposed that this difference is probably caused by a high concentration of planar defects in the low-temperature modification of the Li_2TiO_3 precursor.[23] However, till now there are neither data concerning details of the crystal structure of precursors which present the possibility of an ion exchange reaction nor data concerning the crystal structure of $MO(OH)_2$ (M = Zr, Hf). So far, only a crystallographic study of $TiO(OH)_2$ has been performed. Tarakina *et al.*[23] showed that titanium oxyhydroxide belongs to the family of layered double hydroxides and can be described as a stacking of charge-neutral metal oxyhydroxide slabs $[(OH)_2OTi_2O(OH)_2]$. It possesses a lot of disorder in the structure, partly preserved from the structure of the Li_2TiO_3 precursor.[23,31,32]

The main goal of this study is to solve the crystal structure of the new $MO(OH)_2$ (M = Zr, Hf) compounds using crystallographic information about the related lithium salt, obtained

[a]Institute of Solid State Chemistry, Ural Branch of the Russian Academy of Sciences, 91 Pervomayskaya str, 620990, Ekaterinburg, Russia. E-mail: baklanovay@ihim.uran.ru; Fax: +34 3374 4495; Tel: +34 3374 5219
[b]Kristallographie und Strukturphysik, Universität Erlangen, Staudtstrasse 3, D-91058, Erlangen, Germany. E-mail: Reinhard.Neder@physik.uni-erlangen.de; Fax: +49 9131 8525191; Tel: +49 9131 85251182
[c]Experimentelle Physik III, Physikalisches Institut and Wilhelm Conrad Röntgen – Research Centre for Complex Material Systems, Universität Würzburg, Am Hubland, D-97074 Würzburg, Germany. E-mail: nadezda.tarakina@physik.uni-wuerzburg.de; Fax: +49 9313 184056; Tel: +49 9313 185143

by a citrate synthesis. Our preliminary study and results published by Chai *et al.*[33] show that oxyhydroxides of the 4th group of the periodic table have a high sorption affinity for polyvalent ions, including radioactive ions (Ag, Tl, As, Te, Sr, Th, U *etc.*). Therefore, knowledge of the crystal structure, bond formation, and acid-based properties of oxyhydroxides is essential for understanding the physico-chemical properties of these compounds and will be of help in guiding the design of potential applications.

In addition, the citrate synthesis routine proposed in this work for the synthesis of precursors should lead to a considerable reduction of the synthesis temperature and, probably, the size of the particles in the obtained Li_2MO_3 (M = Zr, Hf) powders which can be interesting not only with respect to the synthesis of $MO(OH)_2$ (M = Zr, Hf). For example, Li_2ZrO_3 was recently proposed as a potential CO_2 absorber material, because of its high capture capacity for carbon dioxide, high stability, and ease of regeneration.[34–40] The need for obtaining this salt with a large surface area (smaller size of the grains) and at lower costs (at lower temperatures) draws the attention to combustion methods for the synthesis of Li_2ZrO_3.[37–41] Li_2HfO_3 is less studied and has been considered as a full structural analogue of Li_2ZrO_3.[28–30] However, in recent work of Baklanova *et al.* the presence of an extra line in the cathodoluminescence spectrum of Li_2HfO_3 obtained by the citrate method has been revealed; this raises the question of there being full structural analogy between the above-mentioned salts or not again.[42]

Experiment

Synthesis

$MO(OH)_2$ (M = Zr, Hf) powders were synthesised from Li_2MO_3 (M = Zr, Hf) precursors by ion exchange reactions.

Synthesis of Li_2ZrO_3 and Li_2HfO_3 precursors. For the synthesis of the Li_2ZrO_3 precursor a stoichiometric amount of $Zr(OH)_2CO_3·5.5–6.0H_2O$ (99.9%) and Li_2CO_3 (99.9%) was dissolved in a nitric acid solution HNO_3 (2 M). The obtained solution was steamed at 250 °C to remove remains of nitric acid. Citric acid ($C_6H_8O_7·2H_2O$) powder was added to the solution, which then was boiled down till the formation of a dry residual solid. Calcination of the precipitate was performed in several steps in the temperature range 300–780 °C with intermediate cooling and regrinding at each stage. Particular details of the synthesis of Li_2ZrO_3 by the citrate combustion method can be found in ref. 43.

Li_2CO_3 (99.9%) and $HfO_2·4.5H_2O$ were used as starting compounds for the synthesis of the Li_2HfO_3 precursor. Initially, fresh $HfO_2·4.5H_2O$ powder was synthesized. For this, HfO_2 (99.9%) was dissolved in a water solution of hydrofluoric acid (40 mass%). The obtained solution was steamed for a long time in order to remove remaining fluoride ions and then diluted 10 times with distilled water. NH_4OH solution (12.5 mass%) was added to the reaction mixture. The latter was kept for 4–5 hours at room temperature in order to reach complete precipitation of Hf ions in a hydrated form. The obtained gel was separated from the solution by decantation, washed several times in distilled water, filtered and dried in air. Then, the freshly synthesized $HfO_2·4.5H_2O$ powder was dissolved in diluted HNO_3 (2 M) with continual stirring and heating at 150 °C; a stoichiometric amount of Li_2CO_3, and an amount of $C_6H_8O_7·2H_2O$ citric acid sufficient for complex formation, were added to the reaction mixture. The obtained solution was then heated at ∼250 °C under constant stirring till the formation of a dry residual solid. Calcining of the residual solid powder was performed in three steps at temperatures of 300 °C (2 hours), 650 °C (10 hours) and 700 °C (4 hours), with intermediate cooling and regrinding in an agate mortar at each stage.

Synthesis of $MO(OH)_2$ (M = Zr, Hf). $MO(OH)_2$ (M = Zr, Hf) oxyhydroxides were synthesised from Li_2MO_3 (M = Zr, Hf) precursors by ion exchange reactions in an acetic acid aqueous solution (0.05 mol l^{-1}) at a temperature of 60 °C during 14 hours. The extent of exchange of Li^+ by H^+ was controlled using a pH-meter (Anion 4100) with a glass electrode. The ratio between solid and liquid phases was 1 g/1 l. The final product, $MO(OH)_2$ (M = Zr, Hf), was washed in distilled water and dried in air till a constant mass was achieved.

Characterization techniques

The elemental compositions of the samples were determined by emission spectral analysis (ESA) using an Optima 4300 DV with inductively coupled plasma (Zr and Hf contents) and by atomic absorption spectroscopy in an acetylene–air flame using a Perkin-Elmer 503 spectrometer (Li content).

X-ray powder diffraction (XRD) patterns were collected at room temperature on a transmission STADI-P (STOE, Germany) diffractometer equipped with a linear mini-PSD detector using Cu $K_{\alpha1}$ radiation in the 2θ range 5°–120° with a step of 0.05°. Polycrystalline silicon (a = 5.43075(5) Å) was used as an external standard. The phase purities of the samples were checked by comparing their XRD patterns with those in the Powder diffraction file – PDF2 database (ICDD, USA, release 2010). The GSAS program package[44,45] was used for structure refinement from powder data.

Synchrotron radiation scattering experiments were carried out at BW5 (DESY, Hamburg, Germany) at a primary energy of 100 keV, *i.e.* a wavelength of 0.123984 Å, using a Perkin-Elmer flat panel area detector at room temperature. The samples were loaded into a capillary with outer diameter equal to 1.8 mm. For background corrections a spectrum from an empty capillary with the same diameter was collected. Refinement of the pair distribution function (PDF) data was carried out with the PDFgui[46] and DISCUS[47] software packages.

The morphology of the obtained powders was studied using a FEI Helios Nanolab Dual Beam system and a JEOL JSM-6390LA scanning electron microscope. Transmission electron microscopy (TEM) studies were carried out using a FEI Titan 80-300 (S)TEM operated at 300 kV. Particle size distributions of the obtained samples were evaluated from SEM images, collected in histogram form and fitted to log–normal distributions.

Nuclear magnetic resonance (NMR) ^{1}H high-resolution spectra were recorded using a Bruker AVANCE AV 300 spectrometer with sample rotation frequency of 18 kHz.

Raman measurements were performed at room temperature on a RENISHAW U1000 spectrometer under Ag^+ laser excitation (λ = 514.5 nm).

For collecting infra red (IR) absorption spectra, powder samples were mixed with caesium iodide (CsI) and pressed into pellets. Spectra were recorded using an IR Fourier spectrometer Vertex 80 (Bruker) in the 400–4000 cm^{-1} frequency range.

Quantum-chemical calculations

Quantum-chemical calculations of monoclinic (sp.gr. $C2/c$) lithium metallates Li_2MO_3 (M = Zr, Hf) were performed using a 24-atom unit cell. Relaxed atomic positions were obtained by minimizing the total energy of the system while keeping the lattice parameters of Li_2ZrO_3 and Li_2HfO_3 fixed at their experimental values (Table 1). The calculations were performed in the framework of density functional theory (DFT) *ab initio* molecular dynamics (MD) with the SIESTA code,[48] where pseudo-atomic orbitals are constructed by means of first-principles norm-conserving pseudopotentials.[49] For the exchange-correlation potential the generalized-gradient approximation in the formulation of Perdew, Burke and Ernzerhof (GGA-PBE) was taken.[50] The calculations of the total energy and of the forces on each atom were performed with precisions of 0.1 meV and 0.5 meV $Å^{-1}$, respectively. For the construction of the pseudopotentials, the following cut-off atomic orbital radii were used: Li (2s) – 2.00 a.u., (2p) – 2.23 a.u.; O – (2s) – 2.00 a.u., (2p) – 1.30 a.u.; Zr – (5s) – 2.00 a.u., (5p) – 3.00 a.u., (4d) – 2.82 a.u. Hf – (6s) – 2.00 a.u., (6p) – 2.78 a.u., (5d) – 2.78 a.u. and for H – 1.25 a.u. All calculations were performed with a double zeta basis set with charge polarisation taken into account and with an energy cut-off of 300 eV. The equilibrium atomic positions were determined by minimizing the total energy by means of the Parrinello–Rahman algorithm.[51]

Results and discussion

Li_2MO_3 (M = Zr, Hf) precursors

In our previous works[21,22] we have shown that the extent of exchange of Li^+ by H^+ for Li_2MO_3 (M = Ti, Zr) compounds obtained by solid state synthesis is significantly higher if the precursors were calcined at lower temperatures. In the present work, Li_2ZrO_3 has been synthesised using citrate synthesis (Table 1).

In both solid-state and citrate synthesis methods a temperature of T = 700 °C was found to be thermodynamically essential for the formation of homogeneous polycrystalline Li_2ZrO_3. However, the application of the citrate synthesis method significantly influences the kinetics of the phase formation, allowing to obtain a Li_2ZrO_3 polycrystalline powder four times faster (Table 1). A noticeable change was also observed in the time required for the ion exchange reaction to complete. Thus, the formation of $ZrO(OH)_2$ takes place three times slower (44 hours) when the precursor prepared by the solid state method is used. For $ZrO(OH)_2$ precursors obtained by the citrate method, complete exchange was observed after 14 hours (Table 1). Taking this into consideration, only precursors obtained by the citrate method have been used for the synthesis of $HfO(OH)_2$.

The morphology of the obtained compounds was studied using SEM and TEM. Li_2ZrO_3 and Li_2HfO_3 obtained by the citrate method contain agglomerates (up to 0.5 μm) typical for combustion synthesis techniques; these agglomerates consist of small lamellar particles with an average particle size of 360 ± 150 nm and 86 ± 37 nm, respectively (Table 1). The value for Li_2ZrO_3 corresponds well with results reported by Xiao *et al.*[40] During the ion exchange reaction, particle size is typically preserved, so that the oxyhydroxides consist of particles of almost the same size and shape as the starting precursors (Table 1, Fig. 1). SEM and TEM images of precursors and oxyhydroxides are shown in Fig. 1.

The XRD patterns of Li_2ZrO_3 and Li_2HfO_3 obtained by the citrate synthesis are shown in Fig. 2. An analysis of systematically absent reflections ($hk0$: $h + k = 2n$; $h0l$: $h = 2n$, $l = 2n$; $0k0$: $k = 2n$) in the XRD patterns indicates two possible space groups, Cc and $C2/c$, for both compounds.

Table 1 Synthesis conditions and crystal structure data of Li_2MO_3 (M = Zr, Hf) precursors and $MO(OH)_2$ (M = Zr, Hf) oxyhydroxides

		Li_2ZrO_3	Li_2HfO_3	$ZrO(OH)_2$	$HfO(OH)_2$
Synthesis conditions	Literature[a]	T = 400 °C, 650 °C; t_{total} ≈ 18 hours[40]	—	—	—
	Present work	T = 300 °C, 650 °C, 700 °C; t_{total} ≈ 16 hours	T = 300 °C, 650 °C, 700 °C; t_{total} = 16 hours	T = 60 °C; t_{total} ≈ 14 hours	T = 60 °C; t_{total} ≈ 14 hours
Particle size		360 ± 150 nm	86 ± 37 nm	400 ± 120 nm	92 ± 35 nm
Crystal structure data	Unit cell parameters[b]	a = 5.4283(1) Å	a = 5.4149(2) Å	a = 5.5996(8) Å	a = 5.5578(5) Å
		b = 9.0297(6) Å	b = 8.9795(3) Å	b = 9.2928(14) Å	b = 9.0701(10) Å
		c = 5.4232(1) Å	c = 5.3991(2) Å	c = 5.6993(8) Å	c = 5.7174(5) Å
		β = 112.72(1)°	β = 112.83(1)°	β = 119.152(9)°	β = 119.746(5)°
	R_{wp}, R_p, $R(F^2)$ (%)	8.14, 6.26, 7.93	8.66, 6.17, 8.25	3.81, 2.86, 0.99	3.64 2.65, 2.45

[a] Literature data in the case of Li_2MO_3 (M = Zr, Hf) are given only for the combustion synthesis method. [b] Li_2MO_3 (M = Zr, Hf) crystallized in sp.gr. $C2/c$, $MO(OH)_2$ in sp.gr. $P2_1/c$.

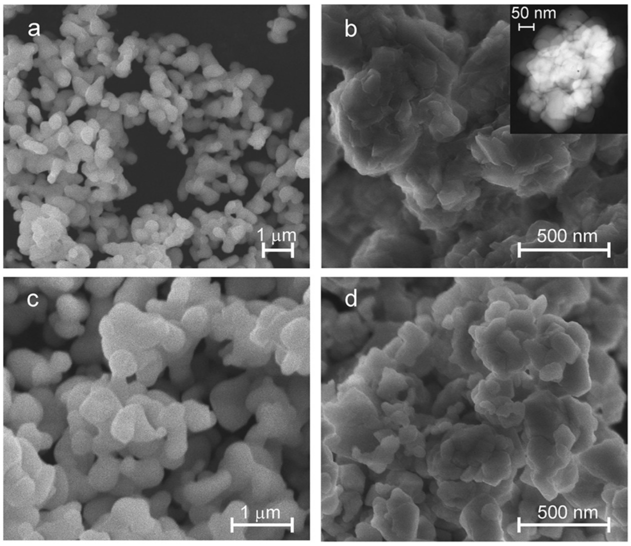

Fig. 1 SEM and TEM images of Li_2ZrO_3 (a) and Li_2HfO_3 (b) precursors obtained by citrate synthesis and $ZrO(OH)_2$ (c) and $HfO(OH)_2$ (d) oxy-hydroxides synthesized from them.

The structure of Li_2ZrO_3 [24] was used as a starting model for the refinement. The peak profiles were fitted with a pseudo-Voigt function, $I(2\theta) = xL(2\theta) + (1 - x)G(2\theta)$ (where L and G are the Lorentzian and Gaussian part, respectively). The angular dependence of the peak width was described by the relation $(\text{FWHM})^2 = U\text{tg}2\theta + V\text{tg}\theta + W$, where FWHM is the full line width at half maximum. The background level was described by a 36-order Chebyshev polynomial. The absorption correction function for a flat plate sample in transmission geometry has been applied. At the final steps of refinement mixed occupancies of the metal sites were introduced. This does not influence the quality of the refinement in the case of Li_2ZrO_3, but considerably reduces the reliability factors for the refinement of Li_2HfO_3. The crystallographic data, *R*-values and selected interatomic distances are given in Tables 1–3.

Li_2ZrO_3 and Li_2HfO_3 salts are isostructural and can be described as a cubic close-packing of oxygen atoms in the octahedral voids between which metals are placed. Only one type of mixed metal layer with a honeycomb arrangement of Li atoms is formed. In the unit cell, two layers are stacked on top of each other along the *c* axis with a 1/6 shift along the *b* direction (Fig. 3).

For both oxides the profile fit of XRD patterns is not perfect: the intensities of some reflections (021, −202, −131, 131, *etc.*) are not described correctly and a non-uniform broadening of the peaks in the 2θ range 18–40° is observed. In spite of a considerable decrease of the *R*-values for Li_2HfO_3 after introduction of mixed occupancies of the metal positions, the above-mentioned issues of profile refinement remain unsolved. Moreover, the chemical composition obtained from the refinement is $Li_{2.04}Hf_{0.96}O_3$, which is different from the nominal one. These facts indicate serious limitations of the presented fit. A more complex approach has to be proposed in order to control the refinement process better, probably the lamellar shape and the small size of the particles have to be included, as well as possible structural defects, as demonstrated for the Li_2TiO_3 compound.[23,31,32]

Similarity in positions and intensity of the lines on the Raman spectra of the Li_2MO_3 (M = Zr, Hf) salts indicates that these compounds are isostructural (Fig. 4). Lines in the spectral range 500–600 cm^{-1} correspond to symmetrical stretching vibrations of Zr–O and Hf–O bonds.[29,30] The ∼14 cm^{-1} shift of Hf–O lines to the high frequency spectral range in Li_2HfO_3 compared with the positions of analogous lines in isostructural Li_2ZrO_3 can be explained by shorter bond lengths in the former (Table 3). Lines at 350–400 cm^{-1} are associated with symmetrical stretching vibrations of Li–O bonds, while lines at 400–500 cm^{-1} and 150–350 cm^{-1} – can be attributed to both stretching and bending vibrations of all M–O bonds.

In order to reveal the chemical bonding characteristics and their dependence on the electronic structure of the M^{4+} ion which forms the salt and on the position of the Li^+ atoms to be substituted by H^+ atoms, *ab initio* calculations have been performed for salts with the following compositions: Li_2MO_3 and $Li_{1.5}H_{0.5}MO_3$ (M = Zr, Hf). The obtained interatomic distances in MO_6 and LiO_6 octahedra for Li_2MO_3 and

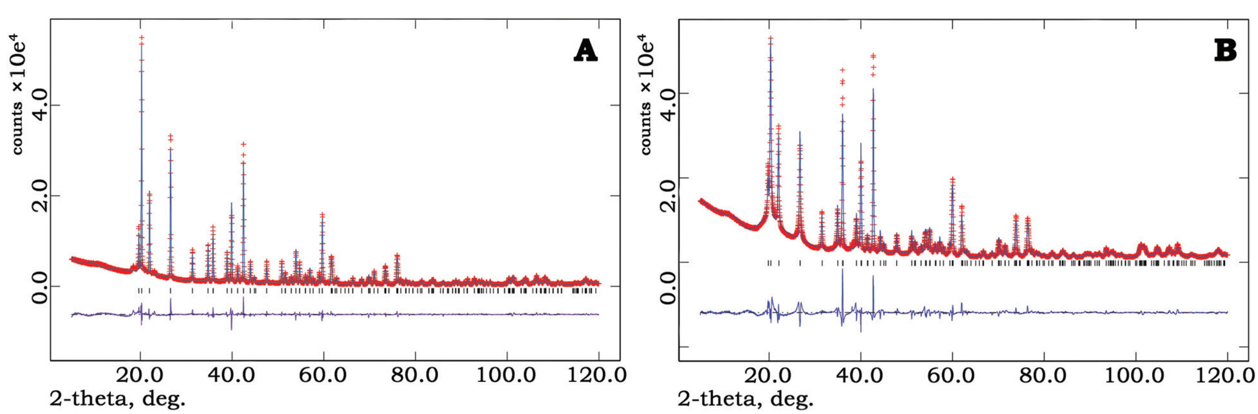

Fig. 2 XRD patterns of (a) Li_2ZrO_3 and (b) Li_2HfO_3 precursors obtained by citrate combustion synthesis.

Table 2 Atomic coordinates and isotropic thermal parameters for Li_2MO_3 (M = Zr, Hf) obtained by citrate combustion synthesis[a]

Atom	x/a		y/b		z/c		Occupancy		$U_{iso} \times 100$ (Å^2)	
M/Li	0		0.09029(16)	*0.08992(26)*	0.25		0.932(8)/0.068(8)	*0.804(9)/0.191(9)*	1.56	*3.18(13)*
Li1/M1	0		0.4208(18)	*0.4167(15)*	0.25		0.974(1)/0.026(1)	*0.886(3)/0.114(3)*	1.76	*3.06(30)*
Li2/M2	0		0.7403(26)	*0.7528(27)*	0.25		1.0/0.0	*0.963(2)/0.037(1)*	2.14	*2.00(60)*
O1	0.25		0.25		0.5		1.0		1.66	*2.5*
O2	0.2732(6)	*0.2790(13)*	0.5743(5)	*0.5711(10)*	0.4841(7)	*0.4913(14)*	1.0		2.23	*2.5*

[a] Data for Li_2HfO_3 are given in *italic*.

Table 3 Selected interatomic distances (Å) for Li_2MO_3 (M = Zr, Hf)

	Li_2ZrO_3		Li_2HfO_3	
Bond	XRD	*Ab initio*	XRD	*Ab initio*
M–O(1) × 2	2.0828(10)	2.0869	2.0739(16)	2.0611
M–O(2) × 2	2.0872(34)	2.1131	2.090(7)	2.0833
M–O(2) × 2	2.106(4)	2.1323	2.039(8)	2.1038
	2.092	**2.111**	**2.067**	**2.083**
	0.008	***0.015***	***0.018***	***0.015***
Li1–O(1) × 2	2.154(12)	2.1808	2.114(9)	2.1585
Li1–O(2) × 2	2.068(12)	2.0580	2.089(12)	2.0364
Li1–O(2) × 2	2.4356(33)	2.3463	2.427(7)	2.3687
	2.219	**2.195**	**2.21**	**2.188**
	0.123	***0.093***	***0.121***	***0.109***
Li2–O(1) × 2	2.2603(9)	2.2291	2.2523(2)	2.2252
Li2–O(2) × 2	2.146(17)	2.2210	2.261(18)	2.2034
Li2–O(2) × 2	2.241(18)	2.1316	2.152(19)	2.1176
	2.215	**2.193**	**2.222**	**2.182**
	0.039	***0.035***	***0.039***	***0.046***

Note: Average values are given in boldface, the relative degree of distortion† of octahedra in italic.

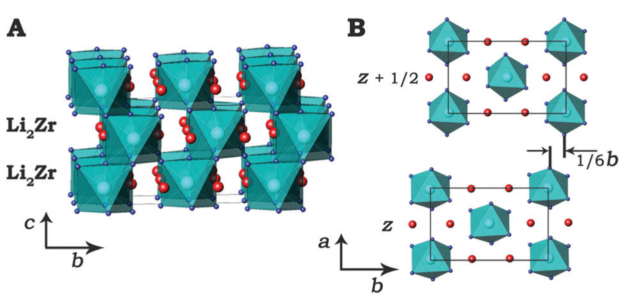

Fig. 3 Crystal structure of Li_2ZrO_3: (a) projection onto the *bc* plane, (b) projection onto the *ab* plane. Li, Zr and O are drawn as red, light-blue and blue spheres respectively.

$Li_{1.5}H_{0.5}MO_3$ are given in Table 3. In both hafnium salts, the calculated M–O distances are shorter and Li–O distances are longer than the corresponding distances in zirconium salts.

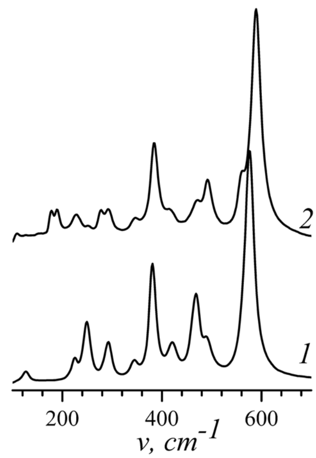

Fig. 4 Raman spectra of (1) Li_2ZrO_3 and (2) Li_2HfO_3.

From XRD and *ab initio* calculations one can conclude that Li1 octahedra are the most distorted ones in both compounds and that, on average, Li_2HfO_3 displays more distortion in polyhedra than Li_2ZrO_3. Substitution of 25% lithium atoms by hydrogen leads to further distortion of MO_6 octahedra (Table 4).

It has been found that H^+ ions which substitute Li^+ to form $Li_{1.5}H_{0.5}MO_3$ salts are considerably shifted from the corresponding Li1 or Li2 positions, which means that one H–O bond in the hypothetic $\{HO_6\}$ octahedra is significantly shorter than

Table 4 Bond lengths in $M^{4+}O_6$ octahedra depending on the atomic position of Li substituted by hydrogen in $Li_{1.5}H_{0.5}MO_3$ (M = Zr, Hf)

	H → Li1		H → Li2	
	M1	M2	M1	M2
Zr–O(1) × 2	2.0346	2.0442	2.1018	2.0472
Zr–O(2) × 2	2.1208	2.0786	2.0706	2.0632
Zr–O(2) × 2	2.1623	2.2325	2.1242	2.2576
	2.1059	**2.1184**	**2.0989**	**2.1227**
	0.0619	*0.0947*	*0.0257*	*0.1104*
Hf–O(1) × 2	2.0062	2.0114	2.0911	2.0302
Hf–O(2) × 2	2.0914	2.0529	2.0376	2.0446
Hf–O(2) × 2	2.1371	2.2075	2.1066	2.2207
	2.0782	**2.0906**	**2.0784**	**2.0985**
	0.0639	*0.0989*	*0.0348*	*0.1011*

Note: Average values are given in boldface, the relative degree of distortion† of octahedra is given in italic.

† The relative degree of the distortion is expressed by $\sigma = \sqrt{\sum_{i=1}^{N} \left|1 - \frac{R_i}{\sum_{i=1}^{N} R_i / N}\right|^2}$ where N is the coordination number (6 for an octahedron), R_i is the metal–oxygen distance.

Table 5 The shortest O–H bond lengths in $Li_{1.5}H_{0.5}MO_3$ (M = Zr, Hf)

	O–H bond (Å)	
$H^+ \rightarrow Li^+$	Li_2ZrO_3	Li_2HfO_3
Li1	1.2482	1.2507
Li2	1.2514	1.2453

the others and probably particularly this bond forms the OH-group (Table 5). Such shift broadens the natural structural channels formed by MO_6 octahedra, which can create a favourable condition for subsequent exchange of Li^+ by H^+.

$MO(OH)_2$ (M = Zr, Hf) oxyhydroxides

The diffraction patterns of $ZrO(OH)_2$ and $HfO(OH)_2$ have been indexed in a $P2_1/c$ monoclinic space group with unit cell constants a = 5.5996(8) Å, b = 9.2928(14) Å, c = 5.6993(8) Å, β = 119.152(9)° and a = 5.5578(5) Å, b = 9.0701(10) Å, c = 5.7174(5) Å, β = 119.746(5)°, respectively. The oxyhydroxides are isostructural. The crystal structure of $HfO(OH)_2$ has been solved using the EXPO2009 program suite.[52] This solution shows that $HfO(OH)_2$ keeps the basic motive of the related Li_2HfO_3 salt.[28] The pairs of Hf octahedra remain preserved in the structure of the oxyhydroxide. However, their rotation in the *ab* plane destroys the oxygen's close-packed arrangement and leads to a lowering of the symmetry of the structure. The obtained model was used as a starting model for the refinement of the crystal structure of both $ZrO(OH)_2$ and $HfO(OH)_2$. It is worth mentioning that the XRD patterns of both oxyhydroxides show significant broadening of Bragg reflections. This broadening can be due to several reasons: lamellar shape of the particles, size of the particles, stacking faults, poor crystallinity, *etc.* In order to describe this broadening, a profile function that employs a multi-term Simpson's rule integration of the pseudo-Voigt function has been used.[44,53,54] Application of this function enables describing the profile when one set of reflections has a different particle size anisotropy than another set. This effect can be found on the diffraction patterns of *e.g.* samples with stacking faults, broadening some reflections and leaving a sublattice of sharp reflections unmodified through the stacking fault. The calculated, observed and difference XRD patterns are shown in Fig. 5. The refined atomic coordinates, temperature factors and selected interatomic distances are given in Tables 6 and 7.

Vibrational spectra of $MO(OH)_2$ (M = Zr, Hf) are given in Fig. 6. Lines at 530–590 cm^{-1}, which correspond to stretching vibrations of Zr–O and Hf–O bonds, split into two components of different intensity. This fact indicates a significant distortion of the MO_6 (M = Zr, Hf) octahedra and an extension of the M–O bonds during the substitution of Li^+ ions by protons in the crystal structure of salts. The Raman spectrum of $HfO(OH)_2$ consists of more splitted lines than $ZrO(OH)_2$, which indicates that the structure of the former is less symmetric. This fact agrees well with crystallographic data obtained from XRD of oxyhydroxides and *ab initio* calculations for partly substituted $Li_{1.5}H_{0.5}MO_3$ phases. Significant broadening of the peaks in the spectrum of $HfO(OH)_2$, in addition to the SEM, TEM and XRD measurements confirms the small particle size of the hafnium oxyhydroxide. The stretching

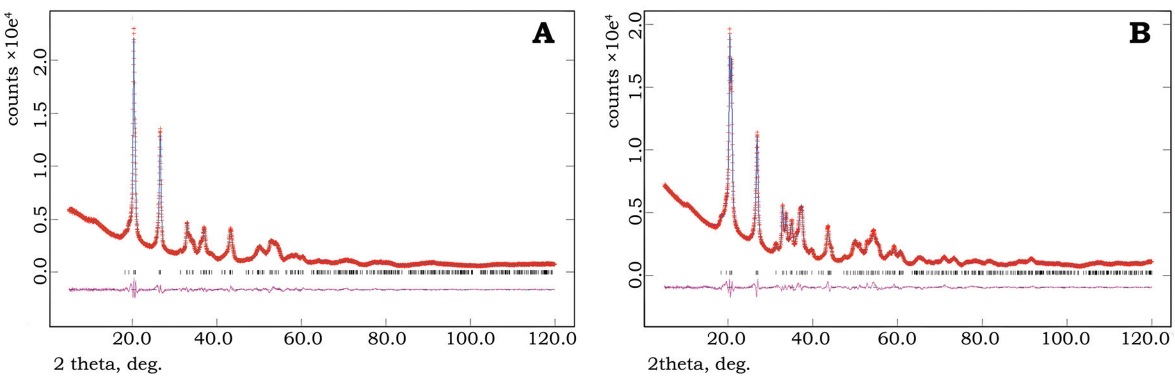

Fig. 5 X-ray powder diffraction patterns of (a) $ZrO(OH)_2$ and (b) $HfO(OH)_2$.

Table 6 Atomic coordinates and isotropic thermal parameters for $MO(OH)_2$ (M = Zr, Hf)

Atom	*x*/*a*		*y*/*b*		*z*/*c*		U_{iso} × 100 ($Å^2$)
M	0.7187(9)	*0.7235(5)*	0.1064(3)	*0.10294(19)*	−0.0315(6)	*−0.04625(35)*	2.50
O1	0.8361(44)	*0.805(4)*	−0.0176(23)	*−0.0658(31)*	−0.2107(35)	*−0.1954(31)*	2.50
O2 (OH)	0.3144(40)	*0.314(4)*	0.0667(21)	*0.0396(22)*	−0.1592(30)	*−0.2279(30)*	2.50
O3 (OH)	0.4890(24)	*0.668(4)*	0.1524(20)	*0.1535(19)*	−0.4821(26)	*−0.4753(40)*	2.50
O4	−0.0286(33)	—	0.2755(18)	—	0.2510(24)	—	2.50

Note: Data for $HfO(OH)_2$ are given in *italic*; occupancies are equal to 1 for all atoms, except for O4 for which it is equal to 0.957(25).

Table 7 Selected interatomic distances (Å) for $MO(OH)_2$ (M = Zr, Hf)

	$ZrO(OH)_2$	$HfO(OH)_2$	
Bond	X-ray	X-ray	PDF
M–O(1)	1.859(20)	1.912(25)	2.231(2)
M–O(1)	2.334(20)	2.302(17)	2.264(7)
M–O(2)	2.045(18)	2.062(19)	2.077(1)
M–O(2)	2.000(15)	2.119(15)	2.126(3)
M–O(3)	2.284(12)	2.362(17)	2.294(6)
M–O(4),*O(3)*	2.2020(15)	*2.294(17)*	*2.112(4)*
	2.121	**2.175**	**2.185**
	0.19	*0.18*	*0.09*

Note: Average values are given in boldface, the relative degree of distortion of octahedral in italic.

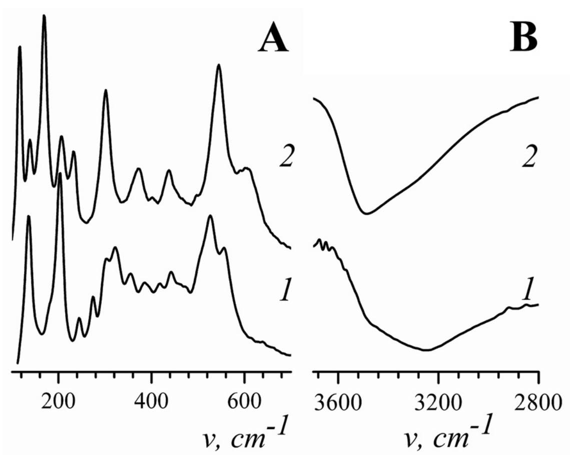

Fig. 6 Raman (A) and IR (B) spectra of (1) $ZrO(OH)_2$ and (2) $HfO(OH)_2$.

vibrations of the O–H bond results in lines in the high-frequency range of the spectra of $MO(OH)_2$ (M = Zr, Hf). The occurrence of broad asymmetric lines at 3400 and 3500 cm^{-1} in the spectrum of $ZrO(OH)_2$ and $HfO(OH)_2$, respectively, indicates the presence of two non-equivalent positions of the OH-groups in the crystal structure.

This fact is additionally confirmed by ^1H NMR measurements, where the ^1H NMR signal of the oxyhydroxides appears as the superposition of two lines with different values of chemical shifts: 6.9, 6.3 ppm and 6.9, 5.9 ppm for $ZrO(OH)_2$ and $HfO(OH)_2$, respectively, indicating two different crystallographic positions of the OH-groups (Fig. 7). Both the smaller value of the chemical shift for $HfO(OH)_2$ and the appearance of lines for stretching vibrations in the high frequency range of IR spectrum point to a stronger base nature of the hydroxyl groups in $HfO(OH)_2$ compared to $ZrO(OH)_2$. Probably, this fact, together with shorter Hf–O bond lengths, allows to conclude that $HfO(OH)_2$ is thermally the most stable among the oxyhydroxides formed by elements of the 4th group (Ti, Zr, Hf) of the periodic table.[21,23] From another point of view, the stronger base nature of the OH-groups in combination with the nanosize of the particles can also be responsible for the much more rapid $HfO(OH)_2$ formation during the ion exchange reaction compared to $ZrO(OH)_2$ (Fig. 8).

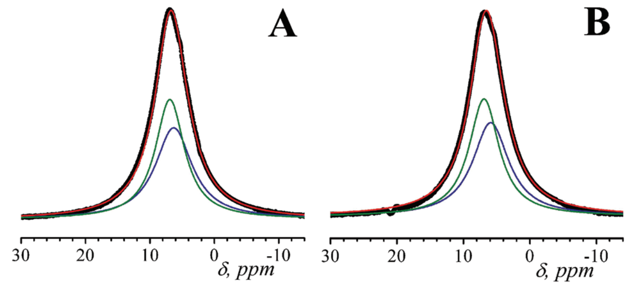

Fig. 7 ^1H NMR (MAS) spectra of (a) $ZrO(HO)_2$ and (b) $HfO(OH)_2$.

Unfortunately, the $MO(OH)_2$ (M = Zr, Hf) oxyhydroxides are not stable under a high voltage electron beam, therefore their local structure cannot be studied directly using transmission electron microscopy techniques. Since $HfO(OH)_2$ was found to be more dispersed than $ZrO(OH)_2$, we tried the same structural models to fit the experimental PDF for $HfO(OH)_2$ in order to get more details on its particle size and its local structure. The PDF technique, similar to the Rietveld refinement, uses a least-squares procedure to compare experimental and model data (PDF) calculated from a proposed structural model. Unit cell constants, atomic coordinates, thermal factors, instrument parameters and the average size of coherently scattering domains (as a spherical particle) have been included in the refinement. The model PDF was convoluted with a Sinc function[55] before comparing with experimental results in order to take into account the finite Q_{max} of the diffraction data.

The model obtained from X-ray powder diffraction data gives a good description of the PDF data in the range r = 1–30 Å, (especially at the r values up to 8 Å, Fig. 9). In order to describe the experimental PDF at higher values of r, a domain size has been introduced into the refinement, resulting in convergence at about 70 Å, but considerably worsening the fit at small r. This fact indicates the presence of disorder, which can be related to the lamellar shape of the particles. It is worth mentioning that the distortion of Hf octahedra was found to be 0.09 from refinement of the whole set of PDF data and 0.19 from the first 8 Å of the pattern, while the value obtained from Rietveld refinement is 0.18 (Table 7). This difference in octahedral distortion indicates that the distortion differs between different domains.

This can be the evidence of size and shape dependence which is described by the PDF analysis more correctly. Summarising, we can say that the presence of disorder in the precursor is most probably retained in the structure of the oxyhydroxide. An additional neutron experiment is essential to get a correct description of disorder and to determine the positions of the hydrogen atoms.

Conclusions

Two new solid oxyhydroxides of the 4th group of the periodic table, $MO(OH)_2$ (M = Zr, Hf), have been synthesised by an ion-

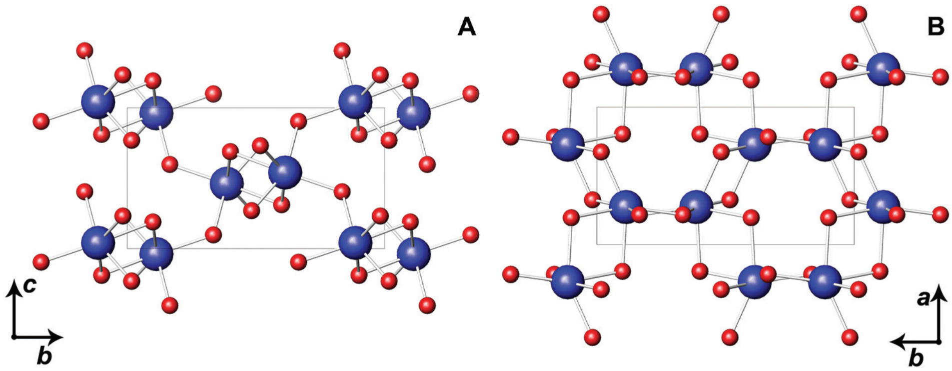

Fig. 8 Crystal structure of $MO(OH)_2$ (M = Zr, Hf), projected onto the *bc* (a) and the *ab* (b) plane. Hf and O are drawn as blue and red spheres, respectively.

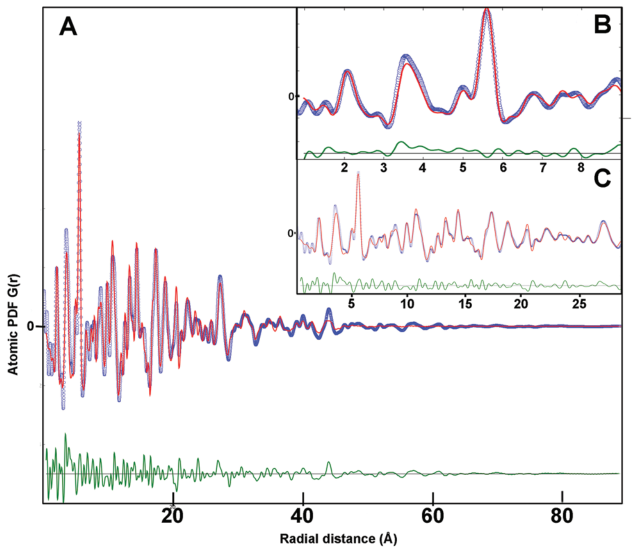

Fig. 9 Experimental (circles) and model (lines) atomic PDFs *G*(*r*) for $HfO(OH)_2$: (a) the whole range, (b) refinement in the range *r* = 1–8 Å, (c) enlargement from (a) in the range *r* = 1–30 Å. The residual difference between the experimental data and the model data is given in the lower part of each plot. The goodness-of-fit is R_w = 26.3%.

exchange reaction from Li_2MO_3 (M = Zr, Hf) precursors and their crystal structure has been solved and refined for the first time. It has been shown that the use of the citrate combustion method for the synthesis of precursors leads to obtaining nano-/sub-micron particles with structural defects; these two factors appear to be essential for completing the process of ion exchange and formation of $MO(OH)_2$ (M = Zr, Hf). Crystal structures of oxyhydroxides keep the basic motif of the related salts and can be described as a framework formed by pairs of edge-sharing MO_6 octahedra connected to each other *via* vertices. XRD, PDF and Raman experiments indicate the presence of two non-equivalent OH groups in the structure and the preservation of structural disorder. However, in order to make a solid conclusion about the origin of the disorder in both salts and oxyhydroxides additional state-of the-art experiments are required. Judging from the value of the chemical shift in NMR spectra and the positions of the lines on IR spectra we can conclude that the acidic nature of structural OH-groups in oxyhydroxides within the 4^{th} group of the periodic table decreases in the series Ti–Zr–Hf.

Acknowledgements

This work was supported by the Russian Foundation for Basic Research under grant no. 12-03-00377 and by the Russian Academy of Sciences (Ural Division) under grant no. 12-M-23-2061 and 13-3-NP-658. N. V. T. acknowledges funding by the Bavarian Ministry of Sciences, Research and the Arts. X-ray powder diffraction studies were carried out at the Center for collective use "X-ray structure analysis" in the Institute of Solid State Chemistry, Ural Branch of RAS (Ekaterinburg, Russia).

Notes and references

1 A. Garcia-Sanchez, E. Alvarez-Ayuso and F. Rodriguez-Martin, *Clay Miner.*, 2002, **37**, 187.
2 S. Brühne, S. Gottlieb, W. Assmus, E. Alig and M. U. Schmidt, *Cryst. Growth Des.*, 2008, **8**, 489.
3 M. Davranche and J.-C. Bollinger, *J. Colloid Interface Sci.*, 2000, **227**, 531.
4 C. Carbone, F. Di Benedetto, P. Marescotti, C. Sangregorio, L. Sorace, N. Lima, M. Romanelli, G. Lucchettiand and C. Cipriani, *Mineral. Petrol.*, 2005, **85**, 19.
5 J. Q. Pan, Y. Z. Sun, P. Y. Wan, Z. H. Wang and X. G. Liu, *Electrochem. Commun.*, 2005, **7**, 857.
6 L. Zhang, Y. Zhong, Zh. He, J. Wang, J. Xu, J. Cai, N. Zhang, H. Zhou, H. Fan, H. Shao, J. Zhang and C.-N. Cao, *J. Mater. Chem. A*, 2013, **1**, 4277.
7 H. Chen, J. M. Wang, T. Pan, Y. L. Zhao, J. Q. Zhang and C. N. Cao, *J. Power Sources*, 2005, **143**, 243.
8 G. X. Do, B. J. Paul, V. Mathew and J. Kim, *J. Mater. Chem. A*, 2013, **1**, 718.

9 A. D. Jagadale, D. P. Dubal and C. D. Lokhande, *Mater. Res. Bull.*, 2012, **47**, 672.
10 M. Casas-Cabanas, J. Canales-Vazquez, J. Rodriguez-Carvajal and M. R. Palacin, *J. Am. Chem. Soc.*, 2007, **129**, 5840.
11 D. S. Kong, J. M. Wang, H. B. Shao, J. Q. Zhang and C. N. Cao, *J. Alloys Compd.*, 2011, **509**, 5611.
12 Y. W. Tan, S. Srinivasan and K. S. Choi, *J. Am. Chem. Soc.*, 2005, **127**, 3596.
13 K. M. Parida, B. Gorai, N. N. Das and S. B. Rao, *J. Colloid Interface Sci.*, 1997, **185**, 355.
14 M. M. Benjamin and J. O. Leckie, *J. Colloid Interface Sci.*, 1981, **79**, 209.
15 Y. Abe, T. Suzuki, M. Kawamura, K. Sasaki and H. Itoh, *Sol. Energy Mater. Sol. Cells*, 2012, **99**, 38.
16 D. D. Zhao, W. J. Zhou and H. L. Li, *Chem. Mater.*, 2007, **19**, 3882.
17 C. Xu, Y. Zeng, X. Rui, J. Zhu, H. Tan, A. Guerrero, J. Toribio, J. Bisquert, G. Garcia-Belmonte and Q. Yan, *J. Phys. Chem. C*, 2013, **117**, 17462.
18 A. Orera, A. Kuhn and F. Garcıa Alvarado, *Z. Anorg. Allg. Chem.*, 2005, **631**, 1991.
19 T. A. Denisova, L. G. Maksimova, E. V. Polyakov, N. A. Zhuravlev, S. A. Kovyazina, O. N. Leonidova, D. F. Khabibulin and E. I. Yureva, *Russ. J. Inorg. Chem.*, 2006, **51**, 691.
20 K. Yawata, *Res. Rep. Tsuruoka Tech. Coll.*, 2006, **41**, 53.
21 T. A. Denisova, *Int. Sci. J. Altern. Energy Ecol.*, 2007, **47**, 78.
22 Ya. V. Baklanova, L. G. Maksimova, T. A. Denisova and N. A. Zhuravlev, *Bull. Russ. Acad. Sci. Phys.*, 2011, **75**, 1118.
23 N. V. Tarakina, R. B. Neder, T. A. Denisova, L. G. Maksimova, Y. V. Baklanova, A. P. Tyutyunnik and V. G. Zubkov, *Dalton Trans.*, 2010, **39**, 8168.
24 J. L. Hodeau and M. Marezio, *J. Solid State Chem.*, 1982, **45**, 170.
25 P. Quintana, J. Leal, R. A. Howie and A. R. West, *Mater. Res. Bull.*, 1989, **24**, 1385.
26 G. Izquierdo and A. R. West, *Mater. Res. Bull.*, 1980, **15**, 1655.
27 J. F. Dorrian and R. E. Newnham, *Mater. Res. Bull.*, 1969, **4**, 179.
28 G. Dittrich and R. Hoppe, *Z. Anorg. Allg. Chem.*, 1969, **371**, 306.
29 N. V. Porotnikov, V. V. Ganin, N. M. Gerardi, L. V. Golubeva and K. I. Petrov, *Russ. J. Inorg. Chem.*, 1987, **32**, 1257 (in Russian).
30 L. V. Golubeva, N. V. Porotnikov, O. I. Kondratov and K. I. Petrov, *Russ. J. Inorg. Chem.*, 1990, **35**, 2604 (in Russian).
31 N. V. Tarakina, R. B. Neder, L. G. Maksimova, I. R. Shein, Y. V. Baklanova and T. A. Denisova, *Z. Kristallogr. Proc. 1*, 2011, 431.
32 N. V. Tarakina, T. A. Denisova, Y. V. Baklanova, L. G. Maksimova, V. G. Zubkov and R. B. Neder, *Adv. Sci. Technol.*, 2011, **63**, 352.
33 L.-Y. Chai, S.-W. Wei, B. Peng and Z.-Y. Li, *Trans. Nonferrous Met. Soc. China*, 2007, **17**, 832.
34 D. J. Fauth, E. A. Frommell, J. S. Hoffman, R. P. Reasbeck and H. W. Pennline, *Fuel Process. Technol.*, 2005, **86**, 1503.
35 E. Ochoa-Fernandez, H. K. Rusten, H. A. Jakobsen, M. Rønning, A. Holmen and D. Chen, *Catal. Today*, 2005, **106**, 41.
36 M. Y. Veliz-Enriquez, G. Gonzalez and H. Pfeiffer, *J. Solid State Chem.*, 2007, **180**, 2485.
37 L. Guo, X. Wang, C. Zhong and L. Li, *Appl. Surf. Sci.*, 2011, **257**, 8106.
38 B. N. Nair, T. Yamaguchi, H. Kawamura, S.-I. Nakao and K. Nakagawa, *J. Am. Ceram. Soc.*, 2004, **87**, 68.
39 B. N. Nair, R. P. Burwood, V. J. Goh, K. Nakagawa and T. Yamaguchi, *Prog. Mater. Sci.*, 2009, **54**, 511.
40 Q. Xiao, Y. Liu, Y. Zhong and W. Zhu, *J. Mater. Chem.*, 2011, **21**, 3838.
41 D. Cruz, H. Pfeiffer and S. Bulbulian, *Solid State Sci.*, 2006, **8**, 470.
42 Ya. V. Baklanova, A. V. Ishchenko, T. A. Denisova, L. G. Maksimova, B. V. Shulgin, V. A. Pustovarov and L. V. Viktorov, *Opt. Mater.*, 2012, **34**, 1037.
43 T. A. Denisova, Y. V. Baklanova and L. G. Maksimova, *R. F. patent*, 2440298, 2012.
44 A. C. Larson and R. B. Von Dreele, Los Alamos National Laboratory Report LAUR, 1994, p. 86.
45 B. H. Toby, *J. Appl. Crystallogr.*, 2001, **34**, 210.
46 C. L. Farrow, P. Juhás, J. W. Liu, D. Bryndin, E. S. Božin, J. Bloch, Th. Proffen and S. J. L. Billinge, *J. Phys.: Condens. Matter*, 2007, **19**, 335219.
47 R. B. Neder and T. Proffen, *Diffuse scattering and defect structure simulation*, Oxford University Press, New York, 2008.
48 J. M. Soler, E. Artacho, J. D. Gale, A. Garcıa, J. Junquera, P. Ordejon and D. Sanchez-Portal, *J. Phys.: Condens. Matter*, 2002, **14**, 2745.
49 N. Troullier and J. L. Martins, *Phys. Rev. B: Condens. Matter*, 1991, **43**, 1993.
50 J. P. Perdew, S. Burke and M. Ernzerhof, *Phys. Rev. Lett.*, 1996, **77**, 3865.
51 M. Parrinello and A. Rahmann, *J. Appl. Phys.*, 1981, **52**, 7182.
52 A. Altomare, M. Camalli, C. Cuocci, C. Giacovazzo, A. Moliterni and R. Rizzi, *J. Appl. Crystallogr.*, 2009, **42**, 1197.
53 C. J. Howard, *J. Appl. Crystallogr.*, 1982, **15**, 615.
54 P. Thompson, D. E. Cox and J. B. Hastings, *J. Appl. Crystallogr.*, 1987, **20**, 79.
55 S. J. L. Billinge, *Local Structure from Diffraction*, Plenum Press, New York, 1998.